Applied Catalysis B: Environmental 304 (2022) 121009

Contents lists available at ScienceDirect

Applied Catalysis B: Environmental

journal homepage: www.elsevier.com/locate/apcatb

Simple modulation of Fe-based single atoms/clusters catalyst with acidic microenvironment for ultrafast Fenton-like reaction

Biao Li [a], Xiaolong Cheng [b], Rusen Zou [a], Xiaoyu Yong [b], Chengfang Pang [c], Yanyan Su [a,*], Yifeng Zhang [a,*]

[a] Department of Environmental Engineering, Technical University of Denmark, DK-2800 Lyngby, Denmark
[b] College of Biotechnology and Pharmaceutical Engineering, Nanjing Tech University, Nanjing 211816, China
[c] Department of Health Technology, Technical University of Denmark, DK-2800 Lyngby, Denmark

ARTICLE INFO

Keywords:
Single atoms and clusters
Advanced oxidation processes
Acidic surface
Flow-through filter
Water treatment

ABSTRACT

Single atom catalysts (SACs) are emerging as efficient peroxide activators to eliminate water contaminants, yet the correlation between structure and catalytic activity remains elusive. Here we moderated the Fe sites on the carbon nitride and obtained a combination of single atoms and clusters sites on $FeCN_5$ with the recorded methylene blue oxidation rate of 59.43 mg/L min^{-1} via direct ultrafast H_2O_2 activation. The excellent performance was mainly ascribed to the high active sites exposure, self-creating acidic microenvironment, and assistance of leaching Fe. Nevertheless, excessive exposure of the catalyst at high pH may destroy the surface environment and inhibit H_2O_2 activation. To solve this issue, we developed a flow-through filter that reached nearly 100% pollutant degradation and H_2O_2 utilization and stability over 320 h when treating actual wastewater treatment. These findings provide profound insights into catalyst manipulation at atomic scales and the development of viable catalytic systems toward real-world application.

1. Introduction

With the growing demand for a healthy living environment, the development of innovative, efficient, and clean wastewater treatment technologies has recently received increasing academic concern. Advanced oxidation processes (AOPs) have been demonstrated as viable technologies to treat wastewater containing toxic and recalcitrant contaminants, taking leverage of reactive free radicals (e.g., hydroxyl radicals, •OH; singlet oxygen, $^1O_2$ and sulfate radicals, $SO_4^{\bullet-}$) released from diverse oxides [1–3]. As the typical first generation of AOPs, H_2O_2-based Fenton process, can degrade rapidly and non-selectively pollutants and ultimately mineralize them into harmless small molecules [4]. However, two scientific challenges have greatly limited its practical application.

One is the efficient utilization of H_2O_2. In the past decades, tons of H_2O_2-activation catalysts have been explored to generate strong oxidative and non-selective •OH [5,6]. Among them, homogeneous catalysts (HoCs) such as iron have attracted tremendous attention for Fenton reaction (Eq. 1) yet suffer from drawbacks of narrow effective pH range, sludge generation, and high-cost recovery processes [7]. To overcome this challenge, heterogeneous catalytic reactions have been comprehensively investigated based on non-precious transition metal (e.g., Fe, Mn, Co, Cu) [8–11] and precious metal (e.g., Au and Ag) catalysts [12,13]. These reactions mainly involve single-electron redox with the participation of metal sites on the catalyst surface [1] (Eq. 2), which facilitate the proposal of the structure-activity relationship. While this relationship is still elusive due to the heterogeneity of active sites with the deviation of catalyst size and variation of exposed active area [14]. Meanwhile, the inherent disadvantage of low H_2O_2 activation efficiency still exists because of the inability of the metal sites inside the catalyst [15].

$$Fe^{2+} + H_2O_2 \rightarrow Fe^{3+} + \bullet OH + OH^- \quad (1)$$

$$M^{n+}{}_{surface} + H_2O_2 \rightarrow M^{(n+1)+}{}_{surface} + \bullet OH + OH^- \quad (2)$$

$$H_2O_2 + \bullet OH \rightarrow H_2O + H_2O \quad (3)$$

Single atom catalysts (SACs), which combine the advantages of HoCs and heterogeneous catalysts (HtCs) and exhibit superb catalytic activity and selectivity, have recently become a research frontier in energy and environmental fields [2,16,17]. With utmost atomic exposure and identical electronic structure, SACs help to establish the deterministic

* Corresponding authors at: Department of Environmental Engineering, Technical University of Denmark, DK-2800 Lyngby, Denmark.
E-mail addresses: yanyansu@daad-alumni.de (Y. Su), yifz@env.dtu.dk (Y. Zhang).

https://doi.org/10.1016/j.apcatb.2021.121009
Received 13 October 2021; Received in revised form 29 November 2021; Accepted 8 December 2021
Available online 10 December 2021

relationship between structure and reactivity [14]. Because of this, single isolated sites were universally found, showing better activity over nanoparticles owing to the maximum dispersion of active sites [14,18]. It is easily neglected that the doping amount of metal needs to be strictly controlled to obtain the single isolate sites. While excessive doping may lead to the aggregation of single sites and the formation of clusters or even nanoparticles, less doping cannot achieves the maximum active exposure due to the large gaps between individual sites [19]. However, only a few studies have focused on the catalytic performance of coexisting single atoms (SAs), single clusters (SCs), and/or nanoparticles [14,15]. Whether there is a balance between SAs and over SA sites for achieving the highest H_2O_2 activation and the respective functions of these sites are still unclear.

The second challenge is the application of catalysts in actual wastewater treatment. Classical HoCs and HtCs are sensitive to harsh environments full of various inorganic ingredients, which undesirably quench reactive radicals and reduce catalytic activity [5,20]. Especially, they do not truly overcome the limitation of narrow pH range and are only applicable in acidic environment [21]. One reason is the formation of iron sludge and the deactivation of •OH under neutral conditions [22]. Another possibility is that the reported wide pH application regions mainly concentrate on the initial value of reaction solutions [6], which would be subject to change during the Fenton process, and could be significantly different from real wastewater with highly uncontrollable pH [21]. Yan et al. reported a cocatalytic heterogeneous catalyst ($CoFe_2O_4/MoS_2$) with an acidic microenvironment for pollutant oxidation, but showed low activity for real wastewater treatment [21]. Therefore, it is urgent and of importance to develop catalysts with high environmental adaptability and vast pH ranges for the large-scale application of Fenton-like reactions in recalcitrait wastewater treatment.

In this study, a Fe-based catalyst with both SAs and SCs was prepared to obtain most exposed active Fe sites by controlling the ratio of carbon nitride (CN) to Fe precursor. The fabricated catalyst indeed exhibited superior activity on H_2O_2 activation and pollutant degradation even under high pH and anion conditions, tackling the two critical challenges encountered by conventional H_2O_2-based AOPs. The reason is that the co-existence of SAs and SCs could create an acidic microenvironment via surface acidity, thereby maintaining the solution pH within the acidic range. This specific function enabled a dual-force catalytic mechanism (surface-mediated catalytic of SAs-SCs sites and homogeneous catalytic of Fe leaching). Furthermore, a novel catalyst modified filter was simply developed and assembled into a flow-through reactor to achieve complete utilization of H_2O_2 for application potential in long-time actual wastewater treatment. Our study presents an evident relationship of structure-reactivity at the atomic level, provides new insights into the rational design of catalysts to truly overcome the harsh environment limitation.

2. Materials and methods

2.1. Chemicals and materials

Chemicals including $FeSO_4.7H_2O$, $FeCl_3.6H_2O$, and urea were used for catalyst synthesis. Methylene blue (MB), meldola's blue (MeB), metyl orange (MO), toluidine blue (TB), orange G (OG), phenol, p-hydroxybenzoic acid (HBA), pyrocatechol (PC), chloramphenicol (CAP), chlortetracycline hydrochloride (CTC) were selected as target pollutants·H_2O_2, potassium titanium oxalate (PTO), ferrozine disodium salt (FDZ), coumarin, NaCl, $NaHCO_3$, K_3PO_4, methanol (MeOH), tert-butanol (TBA), oxalic acid (OA) were used in the catalytic experiments. All reagents were purchased from Sigma-Aldrich without further purification.

2.2. Synthesis of Fe-based catalysts

2.2.1. Homogeneous and heterogeneous catalysts

$FeSO_4·7H_2O$ (4–20 mg/L) and $FeCl_3·6H_2O$ (12 mg/L) were respectively prepared as the homogeneous catalysts. In addition, commercial Fe_2O_3 and classical co-precipitated Fe_3O_4 [23] were used as heterogeneous catalysts.

2.2.2. Modulation of Fe sites on the CN support

The distribution of Fe sites was moderated by increasing the amount of CN support, as illustrated in Fig. S1. Specifically, 0.35 g $FeCl_3.6H_2O$ and different concentrations of urea aqueous solution (0, 0.1, 0.3, 0.5, 0.8 g/mL, 10 mL) were mixed in small-mouth glass vials. These mixed solutions were sonicated for 20 min to ensure the even dispersion of chemicals. Then, the vials were masked by aluminum foil with two fine holes on the mouth, and then were placed into a muffle furnace, heated to 550 ℃ at a rate of 10 ℃/min, and kept at 550 ℃ for 2 h without protective gas. After that, different colors of solids were formed and ground for later use without further chemical treatment.

2.3. Fabrication of catalyst modified filter

Carbon felt (CF) was cut into strips (1 ×5 × 0.5 cm) and then immersed into 1 M H_2SO_4 overnight to remove the impurities on the CF surface. Similar to the procedure in Section 2.2, different precursor solutions were prepared by mixing 0.35 g $FeCl_3·6H_2O$ with urea aqueous solution (0, 0.1, 0.3, 0.5, 0.8 g/mL). Next, the pretreated CF was washed several times with deionized water (DI water) and dried in an oven at 80 ℃. Then it was soaked in the precursor solutions for 5 min. After complete absorption, the wet CF was moved to glass vials and covered by aluminum foil with two fine holes. The vails were then placed into a muffle furnace and underwent the same pyrolysis process. For lab scaled-up experiments, the preparation of the large filter was the same except that CF was cut into pancake-like (4 × 0.5 cm).

2.4. Catalytic experiments

2.4.1. Batch procedure

In a typical experiment, 5.0 mg catalyst was added into MB solution (20 mg/L, 10 mL, pH 7), which were stirred for 10 min to achieve adsorption-desorption equilibrium. The catalytic reaction was started by adding a certain amount of H_2O_2 (50 μL, 17.5 mM) at a rotation speed of 200 rpm. The initial pH of the MB solution was adjusted using 0.1 M HCl or NaOH, and then the pH was measured after adding the catalyst and at the end of the experiment. The effects of H_2O_2 concentration (8.75–35 mM), pH of the solution (3−11), catalyst content (1.0–7.5 mg), and MB concentration (10–40 mg/L) on the treatment performance were investigated, respectively. To keep a constant pH of MB solution, three types of buffer solutions were prepared, including acetic acid-sodium acetate buffer (0.1 M, pH 4), phosphate buffer (0.1 M, pH 7), and boric acid-sodium borate buffer (0.1 M, pH 9). At fixed time intervals, 200 μL solution was taken and mixed with 100 μL MeOH to measure the absorbance of MB solution using Synergy HTX Multi-Mode Reader at wavelength 665 nm. For the degradation of phenolic and antibiotic compounds, 1 mL samples were withdrawn and filtered through a 0.22 μm poly(tetrafluoroethylene) membrane for HPLC analysis (detailed in Table S1). The effects of the water matrix on the degradation of pollutants were performed by directly adding different anions (0.1 M, 100 μL) in various water resources (DI water, tap water, and wastewater). The conditions were similar to the above typical experiment (17.5 mM H_2O_2, 20 mg/L MB, and 5.0 mg catalyst).

2.4.2. Flow through Fenton-filter for wastewater treatment

Two pieces of catalyst modified CF (1 ×5 × 0.5 cm) were filled into a plastic syringe tube (volume of 5 mL) to form a flow-through Fenton-filter. The synthetic MB wastewater (10 mg/L, 1 L, pH 7) was doesed

with H_2O_2 (17.5 mM) and then pumped through the filter. After internal flow-through reactions, the filtrated wastewater was collected and immediately analyzed at a definite time (same as in Section 2.4.1) and then continuously filtrated with a second cycle. All the experiments were performed at room temperature. A reactor was further scaled up to test its practical application potential. Several pieces of modified pancake-like CF (4 × 0.5 cm) were stacked into the middle size of the plastic column (volume of ~220 mL) and connected with a pump. The MB and MO solutions (10 mg/L, 10 L each) at neutral pH were mixed with H_2O_2 (17.5 mM) and then pumped through the reactor, respectively. Subsequently, the mixed solution (10 mg/L MB and 17.5 mM H_2O_2) was directly added into actual wastewater taken from the influent and effluent of wastewater treatment plant (Lyngby, Denmark, detailed in Table S2) without pH adjustment and then filtrated with the same procedure.

2.5. Characterization and chemical analysis

The morphology, structure, and element composition of the catalysts were characterized by scanning electron microscopy (SEM, Quanta FEG 250), transmission electron microscopy (TEM, Tecnai T20 G2) with energy-dispersive X-ray spectroscopy (EDS), and X-ray diffraction (XRD, PANalytical) with Cu Kα X-ray source. The surface chemical states were determined by X-ray photoelectron spectroscopy (XPS, K-Alpha, ThermoFisher), Fourier transform infrared spectroscopy (FTIR, NicoletiS50, ThermoFisher), Zeta potential analyzer (Malvern, ZET-3000HS, UK) and thermogravimetric analyzer (TG, SDT Q600 TA). The Brunauer-Emmett-Teller (BET) specific surface area and pore size distribution of the obtained samples were measured by N_2 adsorption−desorption. Electrochemical analysis was performed by an electrochemical workstation (IVIUMnSTAT) (detailed in Text S1).

The concentration of H_2O_2 was detected by a classical PTO method [24]. The concentration of Fe^{2+} and total Fe was detected by using the FDZ method [25]. Some samples with low concentrations were measured by an inductively coupled plasma optical emission spectrometer (ICP-OES). The generation of •OH was confirmed by the coumarin-fluorescence method (detailed in Text S1). The total organic carbon (TOC) value was analyzed by a TOC-5000 CE analyzer (Shimadzu, Japan).

3. Results and discussion

3.1. Physicochemical characterization of Fe-based catalysts

A series of Fe-based catalysts ($FeCN_x$, x = 0–8) were synthesized via one-pot pyrolysis of mixed precursors containing a fixed content of $FeCl_3$ and different amounts of urea (Fig. 1a). The SEM images exhibit that the uneven Fe particle aggregates disappeared and the morphology of CN

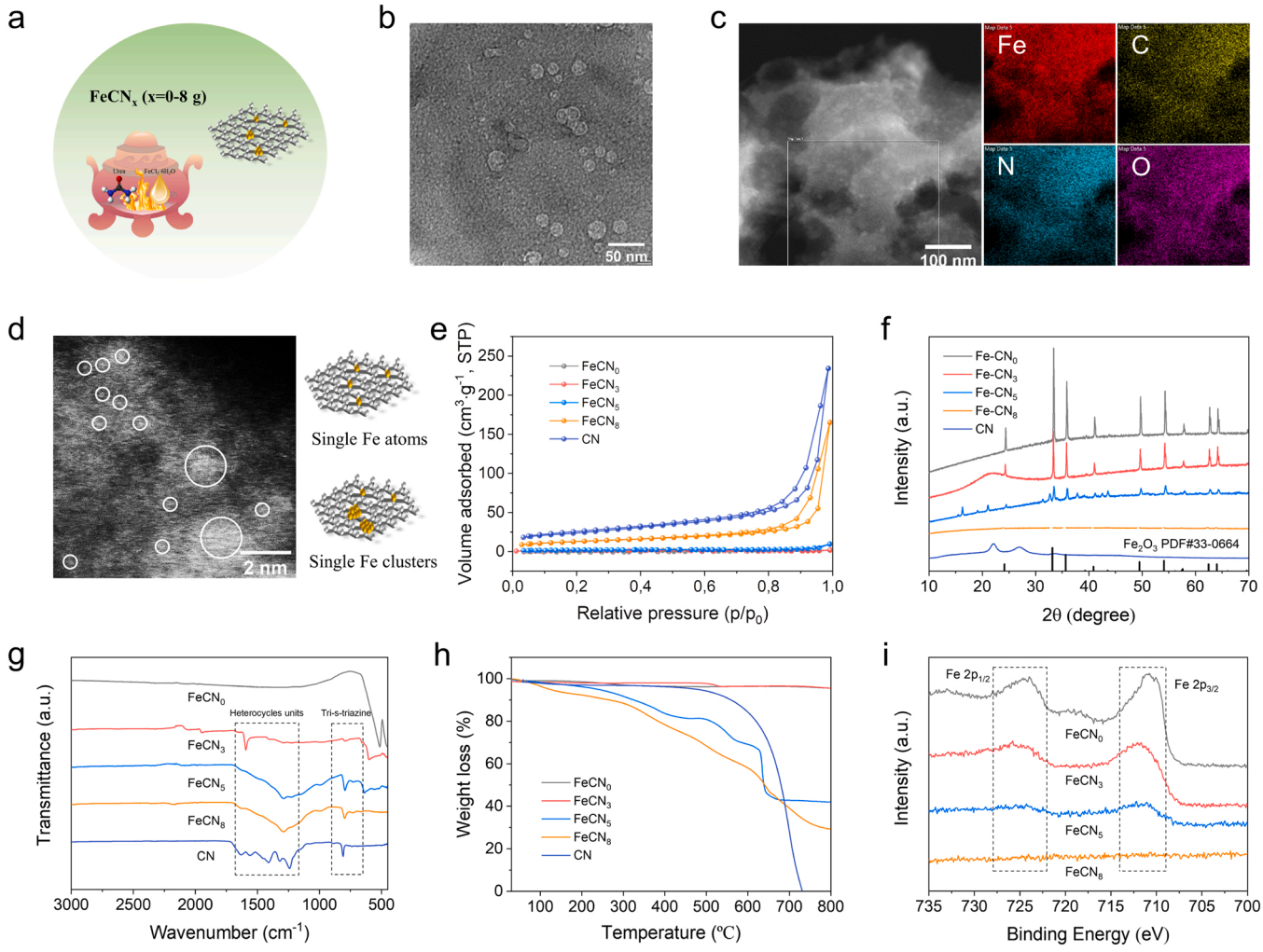

Fig. 1. (a) Illustration of synthesis procedure of Fe-based catalysts. (b) TEM image of $FeCN_5$ with nanopores but no Fe nanoparticles. (c) HAADF-STEM and EDS mapping images of $FeCN_5$ with uniform distribution of Fe, C, N, and O. (d) HAADF-STEM image of $FeCN_5$ and the illustration of single Fe atoms (right-top, corresponding to the small circles) and single Fe clusters (right-bottom, corresponding to the big circles). (e) N_2 adsorption−desorption isotherms; (f) wide-angle XRD patterns (inset of standard peaks of Fe_2O_3); (g) FTIR spectra; (h) TG curves and (i) Fe 2p XPS spectra of Fe-based catalysts.

support was reconstructed from rough stones to smooth shattered tiles with the increased support content (Fig. S2a-d). The gradual dispersion of Fe sites was further confirmed by TEM. The abundant irregularly shaped Fe nanoparticles (5.84 ± 0.82 nm, Table S3) aggregated with the absence of the support (Fig. S2e). While the introduction of trace supports scatteredly anchored less dense particles and reduced their sizes to 3.29 ± 0.44 nm, which was identified as Fe_2O_3 [26] (Fig. S2f). Furthermore, we did not observe prominent black spots on $FeCN_5$ with nanopores and an opaque two-layer edge (Fig. 1b and S2g) and on $FeCN_8$ with a transparent body and jagged rough multilayer edges (Fig. S2h), indicating that the mutual shaping assistance between Fe and CN precursors simultaneously realized the dispersion of Fe sites and effective coarsening of CN support [19]. High-angle annular dark-field scanning transmission electron microscopy (HAADF-STEM) further revealed that four elements (Fe, C, N, and O) were evenly distributed in $FeCN_5$ (Fig. 1c and S3a), and they were similar in intensity tendency but not in values (N > O > C > Fe, Fig. S3b), demonstrating the non-selective isolation of Fe sites by sufficient CN. The reduced intensity of Fe and O in $FeCN_8$ further implying the complete dispersion of Fe sites (Fig. S3c-d). Surprisingly, isolated single Fe dots (small circles) and Fe clusters (big circles) can be seen in $FeCN_5$ (Fig. 1d), while only dispersed dots were obtained in $FeCN_8$ (Fig. S4). It is simulated that the co-existence of SA and SC sites could achieve the highest active Fe exposure by occupying unexploited positions compared with solely SA sites.

The impact of CN support on Fe dispersion was further determined by N_2 adsorption-desorption measurement (Fig. 1e and Table S3). Similar to CN support, $FeCN_8$ possessed a type IV adsorption-desorption isotherms and large BET surface and pore area, reflecting its porous structure in TEM and the weak influence of the highly dispersed SA Fe sites on CN support. In contrast, $FeCN_x$ (x = 0, 3, and 5) showed extremely low BET surface and pore area, presumably because of the condensation destroying caused by the dispersion of Fe guests [19]. XRD spectrum shows that the characteristic peaks of Fe_2O_3 decreased from $FeCN_0$ to $FeCN_8$ (Fig. 1f), confirming the gradual isolation of Fe sites from nano to SA size by CN coordination, most likely in the form of Fe-N bond according to previous reports [14,19]. Moreover, the two identified peaks in CN become invisible in other catalysts, which well matched prior studies and suggested that Fe dispersion could affect the polymerization of CN by disturbing the stacked layer [14]. A similar phenomenon was also found in FT-IR spectroscopy. The featured absorption peaks at 810 and 1650–1200 cm^{-1} in CN progressively declined with the decreasing urea usage, and no peaks of Fe species were displayed (Fig. 1g). The results indicated that Fe interacted with CN support via coordination bonding and inhibited its polymerization process [19,27], which may also benefit -OH group functionalization on the catalyst surface (Fig. S5) [28]. TG analysis demonstrated that the weight loss from 500 ℃ was associated with the decomposition of triazine ring skeletons in CN support [29]. In contrast, the weight loss within 500 ℃ and the stable char yield after 650 ℃ were noticed on $FeCN_5$ but not on CN (Fig. 1h), confirming the disintegration of the CN network and better thermal stability via the Fe sites dispersion.

The surface electronic properties of Fe-based catalysts were investigated by XPS. The percentages of Fe and O both declined, implying that nano Fe_2O_3 was segmented to SA Fe sites as CN support increased, which was also verified by the ICP-OES test (Table S3). Two wide peaks corresponding to Fe $2p_{1/2}$ and Fe $2p_{3/2}$ of Fe species were obtained, which shifted to higher binding energies at higher CN precursor usage (Fig. 1i), implying the valence state change of Fe sites via Fe-N bonding [19]. Further quantitative analysis revealed that Fe^{2+} substantially increased from 25.15% to 61.96% (Fig. S6a), indicating the conversion of Fe^{3+}-N to Fe^{2+}-N species [14]. This conversion is expected to involve pyridinic N, which is the main anchor to isolate Fe sites [30]. As shown in Fig. S6b, three main peaks at 398.7, 399.7, and 400.9 eV were deconvoluted, corresponding to pyridinic N, sp3 tertiary nitrogen N-$(C)_3$, and C-N-H units, respectively [31]. Among them, pyridinic N reached the highest percentage of 39.71% on $FeCN_5$, confirming that the effective combination of SAs-SCs sites formed more active Fe sites. These results demonstrated that CN support successfully dispersed Fe sites from nano to SA scale, reshaped the morphology, structure, composition, and valence of Fe sites, and enhanced its surface area and thermal stability, thereby significantly affecting the catalytic performance of Fe-based catalysts.

3.2. *Ultrafast activation of H_2O_2 for organics oxidation*

3.2.1. *Recalcitrant pollutants degradation*

The efficient H_2O_2-activation by the fabricated $FeCN_5$ catalyst for the degradation of model pollutants was demonstrated. Notably, $FeCN_5$ showed a degradation rate of 59.43 mg/L min^{-1}, which was 20.10, 44.56, and 271.07 folds of that achieved by $FeCN_8$ (SAs), Fe^{2+} (HoC), and $FeCN_3$ (HtC) (Fig. 2a). It was also the highest value recorded so far for MB removal in Fenton-like reactions (Table S4). In addition, the ultrafast complete degradation of MB was achieved by $FeCN_5$ within 20 s (no adsorption observed), while only 89.28% and 5.0% degradation efficiencies were obtained by classical HoCs (Fe^{2+} and Fe^{3+}) after 10 min even with more iron dose (Fig. S7b-c). The classical (Fe_2O_3, Fe_3O_4, and $FeCN_0$ without the CN support) and non-classical ($FeCN_3$ with trace CN support) HtCs all showed negligible degradation efficiencies. To better understand the catalytic performance, the modified concepts of active sites, turnover number (TON), and turnover frequency (TOF) were introduced (detailed in Text S2). The results showed that $FeCN_5$ possessed the most active sites, and its TOF value was 1.01 min^{-1}, which was 8.15–360.71 times higher than other obtained catalysts (Fig. 2b, Table S5). Thus, the activity of these catalytic sites followed the order of SAs-SCs > SAs > HoCs > HtCs. The high activity of $FeCN_5$ was a combination effect of SAs and SCs since individual SAs, HoCs, or HtCs did not show ultrahigh performance.

The pseudo-first-order model (PFO) was further used to assess these oxidation processes (Fig. S8). The $FeCN_5$-catalytic reaction was not well fitted in a positive line (R^2 = 0.74) as the HoCs (R^2 = 0.93) and HtCs (R^2 = 0.99) reactions, suggesting that the mechanism involved in SAs-SCs driven process might be different from the solely HoCs or HtCs-catalytic processes. Moreover, combined with the advantages of high efficiency of HoCs and reusability of HtCs, $FeCN_5$ can be evenly distributed into solutions and easily recovered by membrane filtration, showing excellent activity in different volumes of systems (10–1000 mL) (Fig. S9 and Video S1). To further evaluate the catalytic applicability of $FeCN_5$, multiple environmental pollutants were selected as targets, such as industry dyes (MeB, TB, OG, and MO), phenolic compounds (phenol, HBA, and PC), and antibiotics (CAP and CTC). As expected, all pollutants were efficiently oxidized. The corresponding mineralization efficiencies in 10 min were 55.80–88.55%, 30.23–44.30%, and 38.78–72.16% for dyes, phenolic compounds, and antibiotics, respectively (Fig. 2c). The results demonstrated the non-selective degradation ability and broad applicability of the catalyst.

Supplementary material related to this article can be found online at doi:10.1016/j.apcatb.2021.121009.

3.2.2. *Effects of environmental parameters*

The influences of various factors on MB degradation were systematically investigated, including pH, catalyst content, the concentration of H_2O_2 and MB, different ions, and water sources. As depicted in Fig. 2d, $FeCN_5$ with both SAs and SCs exhibited decreased oxidation efficiency with the initial pH increased from 3 to 11. However, it still maintained at the high values even under alkaline conditions, indicating its strong pH adaptability and substantial superiority over classical Fe-based HoCs and HtCs [6,32]. With the increase of pH, we also observed a decrease in H_2O_2 consumption (63.11–37.65%) and Fe leaching (3.46–2.16 mg/L) (Fig. 2e-f). The established interrelationship between them further indicated the assistant role of Fe leaching in H_2O_2 consumption (Fig. S10a). Comparatively, $FeCN_0$, $FeCN_3$ (HtC), and $FeCN_8$ (SACs) all showed a low concentration of leaching Fe (Fig. S19c).

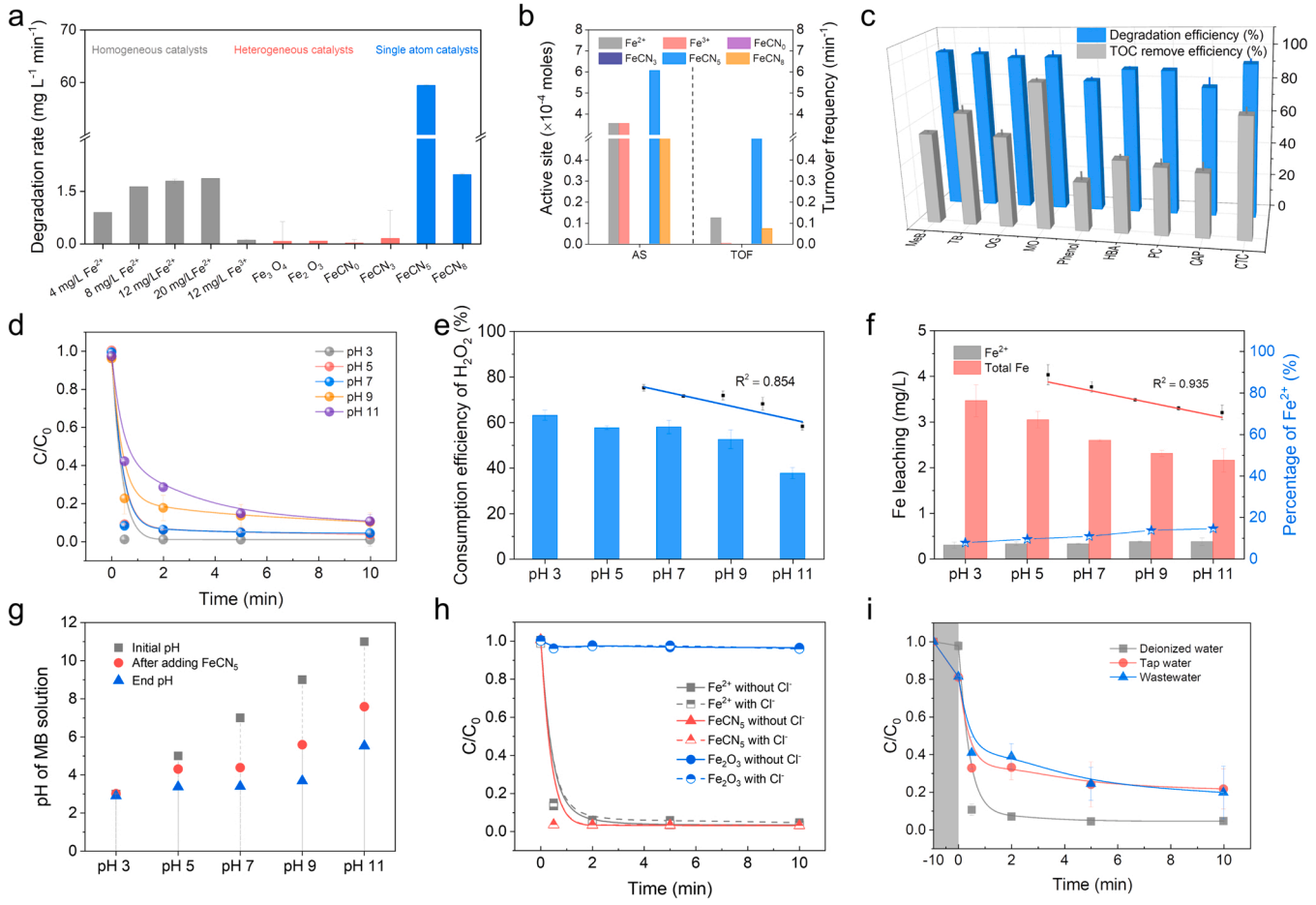

Fig. 2. (a) Degradation rates of MB by H_2O_2 activation with homogeneous catalysts (4–12 mg/L Fe^{2+} and 12 mg/L Fe^{3+}), classical (0.5 g/L Fe_3O_4, Fe_2O_3 and $FeCN_0$) and non-classical (0.5 g/L $FeCN_3$) heterogeneous catalyst, and single atom catalysts (0.5 g/L $FeCN_5$ and $FeCN_8$). (b) Active sites and turnover frequency of Fe-based catalysts. (c) Degradation and TOC removal efficiencies of 20 mg/L dyes (MeB, TB, OG, and MO), phenolic compounds (phenol, HBA, and PC), and antibiotics (CAP and CTC) by the $FeCN_5$-H_2O_2 catalytic system. Influences of initial pH on (d) MB degradation; (e) H_2O_2 consumption, inset of fitted curve of H_2O_2 consumption values under different pH; (f) Fe leaching and the percentage of Fe^{2+} in total leaching Fe, inset of fitted curve of Fe leaching values under different pH; (g) pH changes in the $FeCN_5$-H_2O_2 catalytic system. (h) Influence of Cl^- (1 mM) on MB degradation in the Fe^{2+}, Fe_2O_3, and $FeCN_5$-H_2O_2 catalytic systems. (i) Influence of water sources on MB degradation in the FeCN5-H2O2 catalytic system. Reaction conditions: catalyst (0.5 g/L), MB (20 mg/L), H_2O_2 (7.85 mM) and initial pH (7), if not otherwise specialized.

Thus, the considerable Fe leaching in $FeCN_5$ might be originated from the co-existence of SCs and SAs under acidic pH conditions. To further illustrate the role of leaching Fe (2.60 mg/L) in the $FeCN_5$ catalytic process, we analyzed the homogeneous Fe^{2+} catalytic reaction at the same concentration. As a result, only 18.04% removal of MB was obtained within 20 s, implying that SAs-SCs sites in $FeCN_5$ played a dominant role (i.e., contributed to 81.96% efficiency) in pollutant removal. The weakened catalytic activity of $FeCN_5$ under alkaline conditions was consistent with the increased percentage of Fe^{2+} (or unreacted leaching Fe according to Eq. 1) in the solution.

The high Fe leaching also motivated us to examine the pH changes during the reactions. Interestingly, the pH of the solutions all decreased after $FeCN_5$ addition (Fig. 2g). Primarily, the reduced pH values increased with the increasing initial pH (Fig. S10b). Consequently, the solutions were adjusted naturally by $FeCN_5$ to acidic conditions, providing a preferable pH environment for the Fenton-like reactions [33]. The results demonstrated that $FeCN_5$ with SAs-SCs could overcome the pH limitation and energetically activate H_2O_2 for MB degradation even with alkaline wastewater. Therefore, according to the above findings, the excellent catalytic performance of the $FeCN_5$-H_2O_2 system manifested in multiple pollutants degradation was probably attributed to more active sites, the assistance of leaching Fe, and self-adjusting acidic microenvironment ability of $FeCN_5$.

It is accepted that excessive amount of H_2O_2 could react with •OH and slow down the Fenton process (eq. 3) [34]. A similar result was also found in this work that the degradation rate was slightly decreased with the increased initial H_2O_2 concentration, whereas almost completely degradation was still achieved in all processes within 2 min (Fig. S11). Additionally, H_2O_2 consumption decreased, and Fe leaching increased with the increase of initial H_2O_2 concentration, which was unrelated to the pH changes of the solutions because they showed a similar reduction tendency. The former was probably due to the unfavorable over-utilization of H_2O_2. It was expected that the increase of H_2O_2 would enhance the pollutant degradation as it should induce Fe leaching from the catalyst (2.33–3.85 mg/L). The opposite results observed could support the earlier hypothesis that the ultrahigh activity of $FeCN_5$ was crucially supported by SAs-SCs rather than the leaching Fe.

Meanwhile, we also studied the impact of catalyst content on its catalytic performance (Fig. S12). The results showed that even though the catalyst content was reduced from 7.5 to 1.0 mg, it still maintained almost 100% removal efficiency and a low leaching Fe (1.78 mg/L) below the European Union's environmental regulation (2.0 mg/L) [35]. Especially, we noted that a sufficient amount of catalyst (7.5 mg) with more active sites contributed to the highest H_2O_2 consumption, pH reduction, and least Fe leaching. The removal of high concentrations of MB would require a high amount of •OH participation, thus leading to

increased consumption of H_2O_2 (Fig. S13). However, the change of MB concentration had no evident effect on its "seconds-level" degradation ability due to the ultrahigh efficiency of the catalyst. The Fe leaching and pH changes both showed a stable trend with the shift of MB concentration.

As one of the key factors affecting Fenton reactions, the water matrix may undesirably act as captures to quench •OH with various anions [36]. A key aspect to warrant Fenton's efficiency is the rapid and massive yield of •OH [37]. To this concern, we compared the activities of different types of catalysts under four common ions (Cl^-, HCO_3^-, PO_4^{3-}, and Cr (VI)) in wastewater [38]. Fe_2O_3 showed a negligible effect on MB degradation regardless of the presence of the above anions (Fig. 2h and S14). However, a significant decrease was observed in the Fe^{2+} catalytic process, especially when HCO_3^- or PO_4^{3-} was introduced (reduced by 13.58% and 65.77%, respectively), indicating the yield of •OH was easily disturbed by these anions. It is noteworthy that $FeCN_5$ kept "seconds-level" degradation capability under high concentrations of Cl^-, HCO_3^- and Cr (VI), but displayed the declined efficiency with the additional of PO_4^{3-}. The reasons for this "selective adaptability" was discussed in the following section. Then three types of water sources were selected for MB degradation tests. Fig. 2i shows that a removal efficiency of over 80% was obtained when DI water was replaced by tap water and wastewater, even though complex components affected the adsorption and degradation processes (Table S2). Overall, the unique structure of $FeCN_5$ endowed its outstanding activity and adaptability against various wild water chemistry.

3.3. Catalytic mechanisms

3.3.1. Identification of active sites and involved radicals

Unlike the HoCs and HtCs catalytic processes, $FeCN_5$-based Fenton reactions can be well divided into two stages (Fig. S15). Benefiting from the ultrahigh activity of $FeCN_5$, the slopes in the first stage (0–0.5 min) were all significantly higher than that of the second stage (0.5–10 min). We also noticed that the first-stage slopes were also higher than the slopes achieved by homogeneous (Fe^{2+} and Fe^{3+}) and heterogeneous (Fe_2O_3 and Fe_3O_4) catalysts, which affirmed the "seconds-level" oxidation ability of $FeCN_5$ with the co-existence of SAs and SCs. Given this result, we further adopted the Langmuir-Hinshelwood model (L-H) to describe the surface-mediated catalytic process (SMC) associated with molecules adsorbed on surface-active sites [39]. Accordingly, H_2O_2 and MB are two key molecules that may be involved in this work. The correlation between K and the concentration of H_2O_2 or MB can be fitted to a line, and the slopes were estimated to be 0.635, and 0.889, respectively (detailed in Text S3). It demonstrated that the $FeCN_5$-based Fenton reactions involved the SMC, in which H_2O_2 and MB might be adsorbed on the SA-SC Fe active sites in a self-adjusted acidic environment. The fitted PFO curves in the HoCs and HtCs catalytic processes did not follow a surface-based process due to the absence of active Fe sites on the support surface. Furthermore, the electron transfer between the two molecules and the active sites was tested by chronoamperometry (i-t curve), which could also verify the contributions of radical and non-radical pathways during this process (Fig. 3a) [40]. When H_2O_2 was injected into the three-electrode system, the control (without any catalyst) and $FeCN_0$ had no current responses. In contrast, an apparent current jump appeared on $FeCN_3$, $FeCN_5$, and $FeCN_8$, and the highest current peak was obtained on $FeCN_5$. Afterward, the introduction of MB did not lead to a distinct current response on the above catalysts. On the one hand, it implied that electrons were transferred from the Fe sites to the surface-adsorbed H_2O_2 for radical generation, among which $FeCN_5$ showed outstanding performance due to its highest Fe active exposure [41]. On the other hand, MB degradation mainly occurred in a radical pathway instead of the non-radical pathway. Considering the assistant role of high leaching Fe, we can further speculate that an HoC-SMC dual-driving mechanism could be achieved via associating the induced HoC reactions. To confirm the presence of reactive sites, we introduced oxalate as a chelator of Fe sites into the catalytic system (Fig. 3b). The MB oxidation was suppressed from 100% to 50.23% with the increased

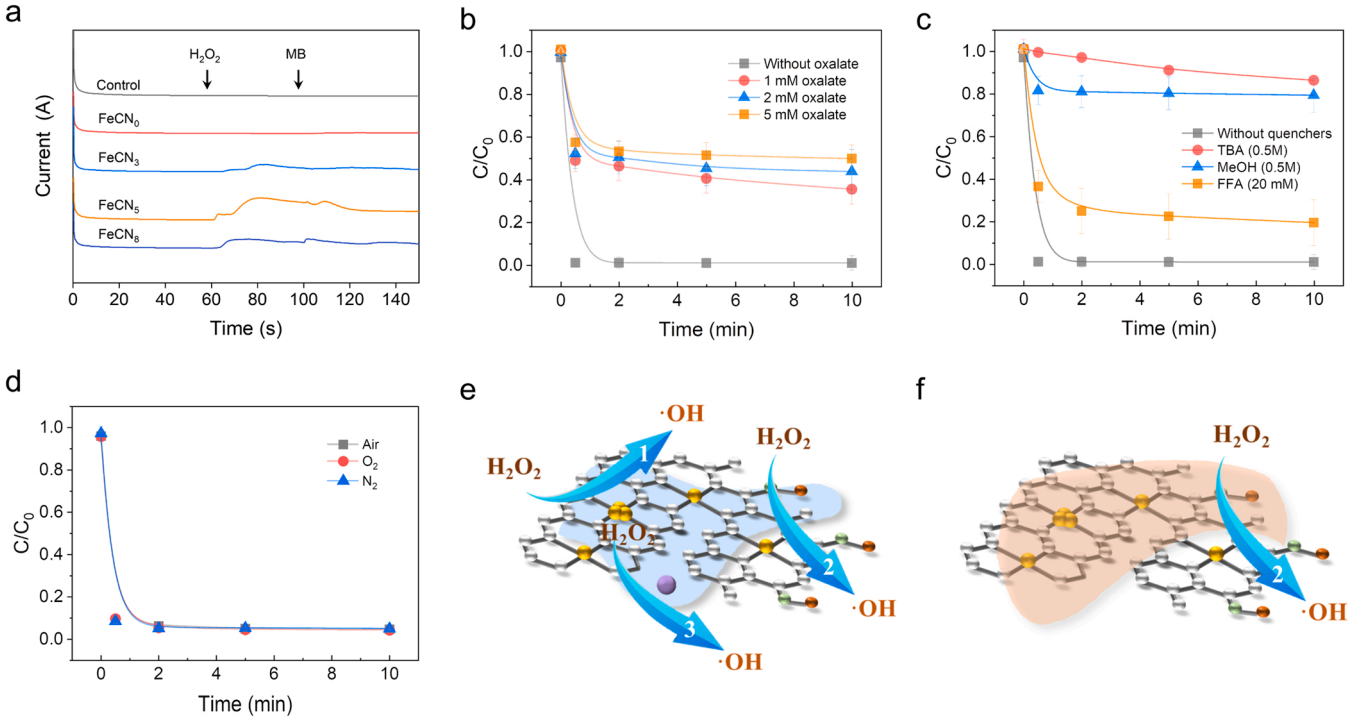

Fig. 3. (a) Chronoamperometry test of Fe-based catalysts with the addition of H_2O_2 and MB, respectively; the glassy carbon electrode coated with Fe-based catalysts, Pt foil, and Ag/AgCl electrode were used as the working, counter, and reference electrode, respectively. (b) Influences of oxalate; (c) quenching reagents and (d) gases-saturated solutions on MB degradation. Proposed mechanisms of the $FeCN_5$-H_2O_2 catalytic system for •OH generation (e) without and (f) with the high pH buffer solution. Reaction conditions: $FeCN_5$ (0.5 g/L), MB (20 mg/L), H_2O_2 (8.75 mM), and initial pH (7).

oxalate concentration, demonstrating the central role of Fe sites [42]. However, the SMC reactions still acted as a governor even part of the Fe sites might be deactivated on the catalyst surface (Fig. S16c).

To recognize the contributions of free radicals in the $FeCN_5$-catalytic process, we employed MeOH, TBA, and FFA as chemical probes to detect •OH, $SO_4^{\bullet-}$, and $^1O_2$, respectively [43]. The addition of 0.5 M MeOH or TBA severely impacted MB oxidation, reducing degradation efficiencies from 100% to 20.64% and 13.63%, respectively (Fig. 3c). The results suggested the dominant role of in situ-produced •OH during this process. A minor adverse effect caused by FFA could be due to its relatively low reactivity with •OH (1.5×10^{10} M^{-1} s^{-1}) [43]. Meanwhile, the yield of •OH was not derived from the activation of dissolved O_2 because the same efficiency was obtained in varying gases-saturated solutions (Fig. 3d). More importantly, the two-stage linear curves were still well fitted, which demonstrated that these chemicals only served as radical scavengers but did not intervene in the SAs-SCs mediated H_2O_2 activation processes (Fig. S16d).

3.3.2. *Acidic surface for pH adjustment*

The relationship between activity and the acidic surface of $FeCN_5$ was illustrated by comparing the changes in degradation activity, pH, and •OH concentration in different solutions. When we used DI water (initial pH 7) as the solution, $FeCN_5$ was discovered to be the most catalytically reactive to drive H_2O_2 decomposition and MB degradation compared to $FeCN_0$, $FeCN_3$, $FeCN_8$ (Fig. 4a). This advantage was clearly confirmed by the difference of •OH-fluorescence intensities (FI, Fig. 4b). The solution was then replaced by acetate buffer (pH 4) to ensure a stable pH throughout the process (Fig. S17e). Fig. 4c shows that the catalytic activity of $FeCN_5$ was severely inhibited, as suggested by the reduced degradation efficiency (100–27.47%) and rate (39.57–0.549 mg/L min^{-1}). A similar decrease tendency was also reflected in other types of catalysts due to the lack of vitality in •OH generation (Fig. 4d). The high Fe leaching (2.94 mg/L) indicated that the HoC catalytic process might not be restrained in this buffer solution (Fig. S17f). Hence, the reduced •OH may be related to the suppression of the SMC process or the quenching effect of acetate buffer [44]. Inspired by this interesting phenomenon, we explored the influences of other buffer solutions on $FeCN_5$ activity. Not surprisingly, when phosphate buffer (pH 7) was prepared as the solution, the FI of •OH was further subsided, and the discrepant catalytic performance between these catalysts was not obvious within 10 min (Fig. S17a-b). Remarkably, their degradation capabilities were almost entirely impeded because the signals of •OH all disappeared if we introduced borate buffer (pH 9). The calculated TOF results further proved the inhibited catalytic activity. The value drops from 1.01 to 0.0023 min^{-1} (Table S6), which could be due to the formation of surface metal-OH complexes at higher pH values and the repelling of H_2O_2 from exposed active sites [45]. Interestingly, we noticed that the catalytic reactions that participated in these processes might be changed if we used buffer solutions (Fig. S18). In detail, the two-stage curves were retained for the SMC process in pH 4 buffer solution. Still, the process was severely limited under pH 7 buffer solution and almost completely inhibited under pH 9. Thus, the potential mechanisms for the activation of H_2O_2 could include both the SAs-SCs sites and the Fe leaching from the SAs-SCs sites (Fig. 3e). The buffer solutions might create a stable pH around the catalyst surface, making it impossible for the catalyst to self-regulate and maintain the acidic microenvironment and reaction sites (Fig. 3f). Furthermore, the destroyed surface environment could result in the looting of active sites for H_2O_2 landing [45]. Consequently, the Fenton-like process cannot proceed efficiently via the SMC, becoming the rate-determining step of surface reactions. In addition, the role of leaching Fe in H_2O_2 activation was weakened since its concentration decreased from 2.60 to 0.03 mg/L using the buffer (Fig. S17f). Therefore, the dual-driving force for activating the H_2O_2-based Fenton reactions was severely disabled.

To further illustrate the pH-adjusting property of $FeCN_5$, a series of experiments were conducted. Firstly, we tested H_2O_2 consumption, pH changes, Fe leaching of other obtained catalysts for comparison. Taking the advantages of SA-SC sites, high Fe leaching, and self-created acidic microenvironment, $FeCN_5$ possessed extraordinary activity compared with HoC (Fe^{2+} and Fe^{3+}) and HtC ($FeCN_0$ and $FeCN_3$) (Fig. S19a). In contrast, with high utilization of 96.97%, Fe^{2+} only contributed 41.23% of H_2O_2 consumption in the homogeneous Fenton process (Fig. S19b). In the end, a high concentration of Fe^{3+} remained as residual sludge since it cannot be restored to Fe^{2+} for H_2O_2 activation [46] (Fig. S19c). More

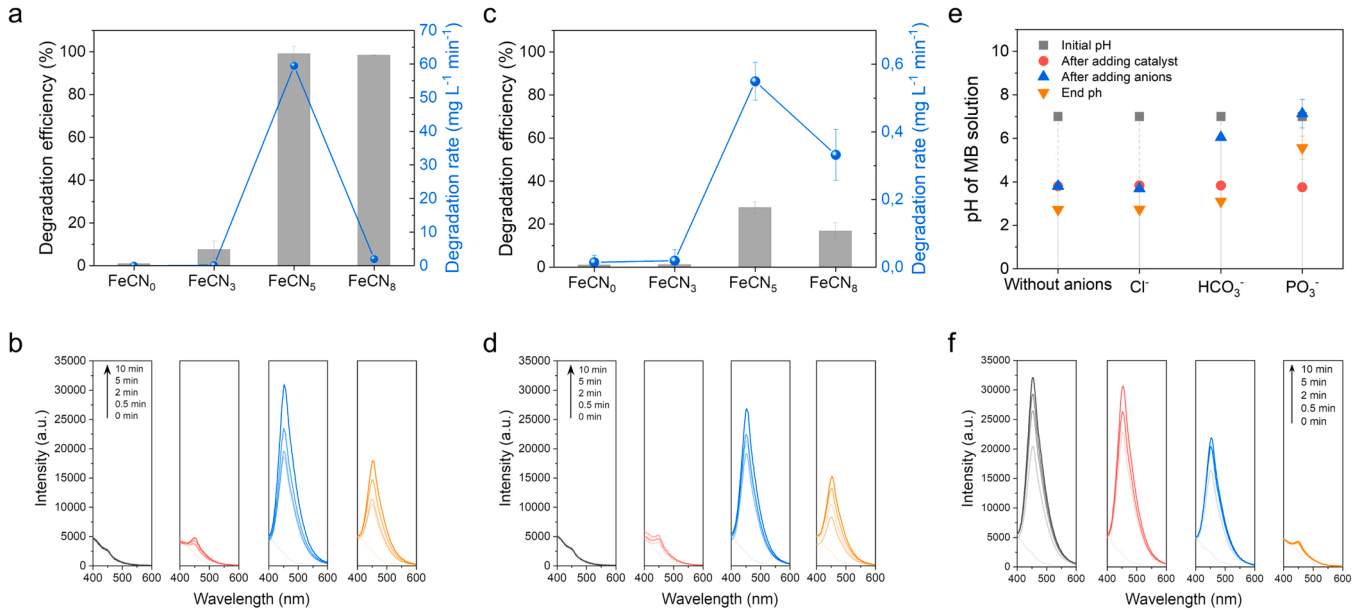

Fig. 4. (a) Degradation efficiencies and rates of MB; and (b) •OH accumulation in the Fe-based catalyst-catalytic system without buffer solutions. (c) Degradation efficiencies and rates of MB; and (d) •OH accumulation in the Fe-based catalyst-catalytic system with acetate buffer solution (pH 4). (e) pH changes; and (f) •OH accumulation in the $FeCN_5$-H_2O_2 catalytic system with and without the existence of anions. The grey, red, blue, and orange curves in (b, d, and f) indicate $FeCN_0$, $FeCN_3$, $FeCN_5$, and $FeCN_8$, respectively. Reaction conditions: MB (20 mg/L), catalyst (5 mg), H_2O_2 (8.75 mM), buffer (0.1 M), and anions (1 mM).(For interpretation of the references to colour in this figure, the reader is referred to the web version of this article.)

importantly, pH was stable during this classical reaction (Fig. S19d). The same trend was also observed in the Fe^{3+} and $FeCN_0$ catalytic processes. However, we noticed that with the support of CN, $FeCN_3$ and $FeCN_8$ were also endowed with the pH-adjusting ability, which significantly reduced the pH from 7 to 3.80 and 5.54, respectively. In addition, we measured the zeta potential of these catalysts. With the support of CN, $FeCN_x$ ($3 \leq x \leq 8$) all showed positive zeta potential (initial pH 7). Specifically, with the increase of the support content, the zeta potential of the catalysts increased from 22.63 to 45.93 mV, indicating the decrease of acidity of the catalysts. (Fig. S20a). This result was consistent with the pH changes of these catalysts observed during the experiment [21]. In this case, the surface acidity helped to create an acidic environment on the catalyst surface. This unique property might be associated with the high condensation destroying CN by Fe dispersion (Fig. 1 and S5). Consequently, the inability of $FeCN_3$ could be owing to the lack of the active Fe sites on the catalyst surface and sufficient Fe^{2+} from Fe leaching (Fig. S19b), which are essential for H_2O_2 activation.

Secondly, we explained the selective adaptability of $FeCN_5$ under different conditions. As we mentioned that the activity of $FeCN_5$ was hindered with the existence of PO_4^{3-}, and in tap water and wastewater. This selective adaptability was tightly bound to the pH condition of the solution because the reduced pH returned to the initial value of 7.0 after the addition of PO_4^{3-}, damaging the acidic environment of the $FeCN_5$-H_2O_2 system (Fig. 4e). Apart from pH changes, Fe leaching, an assistant for H_2O_2 activation, was also significantly suppressed by 5-fold (Fig. S19e). Therefore, the accumulation of •OH could be solid evidence of the inhibited capabilities above (Fig. 4f). Similarly, when tap water and wastewater were used as the solutions, the pH only drops slightly after the catalyst was added, showing that the higher alkalinity solutions are less prone to be acidified by the inhibited pH-adjusting ability (Fig. S19f) [21]. Comparatively, this excellent ability enabled $FeCN_5$ to be applied to different volume systems, achieving efficient pH reduction (even in three cycles) and H_2O_2 utilization in DI water without buffering properties (Fig. S20b-d). In conclusion, the accumulation of •OH in the $FeCN_5$ catalytic process was markedly interfered by the pH conditions of the solutions, other than the existence of background organic and inorganic substances commonly found in water.

3.4. Flow-through Fenton filter toward practical application

Microfiltration is known as one of the effective strategies in real wastewater treatment [47,48]. To increase the lifespan and reusability of $FeCN_5$ for water purification, a flow-through Fenton filter that integrated $FeCN_5$ and CF was developed (Fig. S21a-b). Other catalysts were also combined with CF for comparison. With $FeCN_5$-modified filter, the device achieved over 90% removal efficiency in a single-pass mode at the flow rate of ~100 mL/h (Fig. 5a). We also noticed that H_2O_2 utilization was reduced from 93.07% to 79.58% after 10 h, indicating that the system did not require much H_2O_2 as the free catalyst. Then we performed a second filtration to flow the filtrated synthetic MB wastewater through the filter again without adding H_2O_2. It can be seen that the wastewater was completely colorless (Fig. S21b), and H_2O_2 was also completely utilized. More importantly, the filter energetically maintained both high degradation (97.49%) and H_2O_2 utilization efficiencies (95.99%) after three cycles (Fig. S21d). However, this excellent reusability did not occur in the batch catalytic experiments because the aggregated catalyst fully immersed in the solution might limit its surface availability and poison the reaction sites (Fig. S9a) [49]. The control experiments performed with a bare CF exhibited a negligible catalytic performance by mixing H_2O_2, delivering poor adsorption of CF and low oxidizing power of H_2O_2 in this flow mode. When CF was decorated with different catalysts, we observed varying degradation efficiency in the order of $FeCN_8$/CF > $FeCN_3$/CF > $FeCN_0$/CF (Fig. S21c), which was consistent with the performance of individual catalysts dosed directly into the water as shown in Fig. 2a. Note that these catalyst-modified filters were either inefficient or unstable for water treatment.

The flow-through Fenton filter was further scaled up to 10 L and tested with a fast flow rate of ~250 mL/h to explore its scale-up potential in actual wastewater application (Fig. 5b). The large filter was prepared by irregularly coating $FeCN_5$ on the surface of each carbon felt (Fig. 5c). Without external pressure equipment, the wastewater passed through the filter under gravity (Fig. 5d). As expected, high MB degradation and H_2O_2 utilization efficiencies were obtained with the same synthetic wastewater during the first filtration process, but both were slightly reduced after 40 h (Fig. 5e). In the second filtration cycle, the efficiencies were enhanced to nearly 100% while H_2O_2 utilization

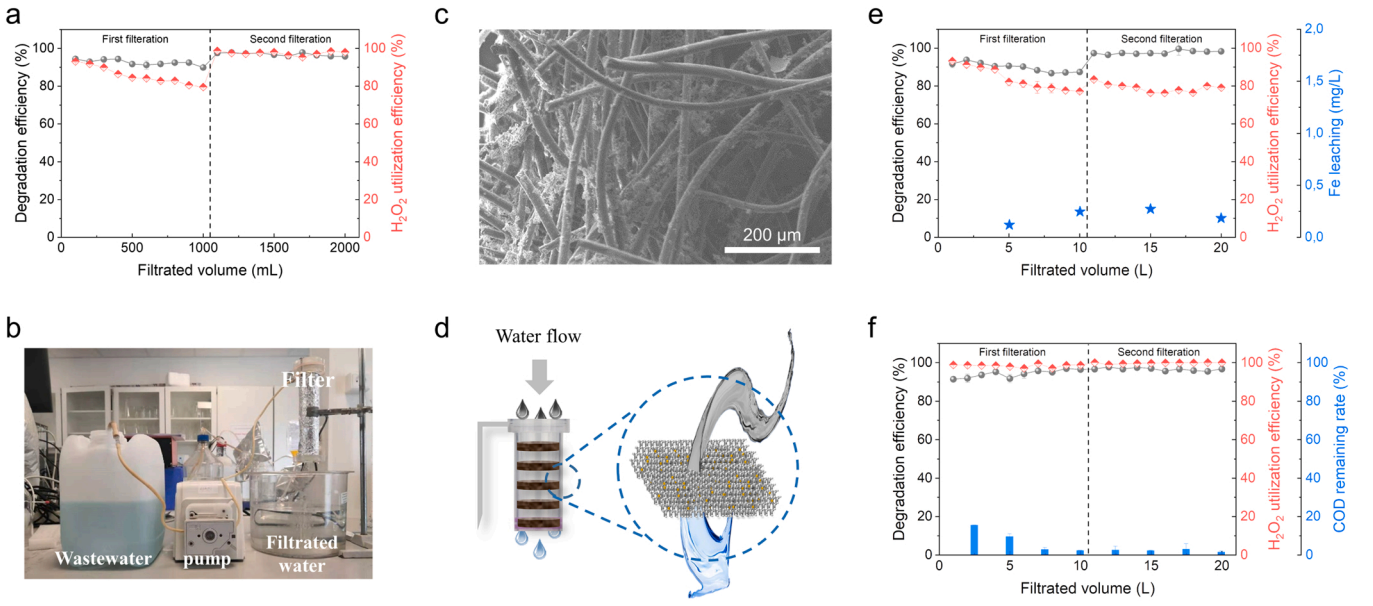

Fig. 5. (a) MB degradation (10 mg/L) and H_2O_2 utilization efficiencies (initial concentration of 7.85 mM) by a small size of filter (5 × 1.5 cm out diameter) at a flow rate of ~100 mL/h. (b) Image of a flow-through device assembled with a middle size of filter (22 × 4 cm out diameter). (c) SEM image of the filter coated with $FeCN_5$ catalyst. (d) Schematic of the gravity-driven filter for wastewater filtration. (e-f) MB degradation and H_2O_2 utilization efficiencies by a middle size of filter at a flow rate of ~250 mL/h. Fe leaching in the filtrated wastewater were recorded in (e) and (f), and COD remaining rates of effluent wastewater (initial concentration of 52.62 mg/L) were shown in (f).

remained unchanged. It might be due to the higher flow rate leads to shortened contact time among H_2O_2 molecules, catalyst surface, and organic pollutants, while the limited time was still sufficient for removing MB [12]. Moreover, we detected the relatively low Fe leaching (< 0.5 mg/L) during the whole process, indicating that the present filter design was beneficial to reduce Fe leaching. At 40 h, we changed the simulated MB wastewater to 10 mg/L MO wastewater to test the applicability of the filter for eliminating different pollutants (Fig. S22b). Similar tendencies in degradation and H_2O_2 utilization were obtained, where the filter not only achieved the complete removal of 10 L MO at the end, but also with the extremely low Fe leaching (< 0.2 mg/L) in the effluent, confirming its high activity and stability (Fig. S22d).

We finally challenged the efficacy of the filter to treat real effluent and influent wastewater spiked with MB. As we discussed that $FeCN_5$ exhibited decayed degradation activity due to the destruction of the acidic environment by the high alkalinity of the tested wastewater (Fig. 2h). However, this challenge was significantly alleviated by this flow-through Fenton filter. As shown in Fig. 5f, MB degradation and H_2O_2 utilization presented almost a coincide line with ~100% efficiency. The enhanced H_2O_2 consumption was likely to attribute to the oxidation of a wide variety of organic molecules according to the low COD level during the process. Note that the performance of the filter was not inhibited by the existence of various anions in high pH wastewater (Table S2), which demonstrated that $FeCN_5$ reside inside the filter could reduce the unnecessary long-term exposure to the external constituents thereby keeping a high reactivity. The extremely low concentration of Fe (< 0.01 mg/L) in the filtrated water could also be reasonable evidence for this reduced exposure (Fig. S22g). The influent wastewater with a high concentration of COD and anions was subsequently filtrated through the filter (Fig. S22e)·H_2O_2 was completely utilized during the two consecutive filtration processes within this more complex environment, whereas the COD removal efficiency decreased to 49.42–74.83%. The reduction of removal efficiency was not caused by Fe deactivation as Fe leaching was low (Fig. S22h). After adding more H_2O_2, the removal efficiency was significantly improved (Fig. S22i). It should be noted that the degradation efficiency decreased a bit in the first 20 h. Still, it can be rapidly recovered and stably maintained at 100%, suggesting the long-term stability of the filter. The SEM image of the filter further confirmed this after filtration, where a similar amount of catalyst aggregation can be seen across the CF before and after the water treatment (Fig. S22f). Therefore, the flow-through Fenton filter showed high utilization of H_2O_2, ultrahigh catalytic efficiency, low energy consumption, and long-term stability and posed the scaling-up potential for the treatment of different wastewater pollutants.

4. Conclusions

This study revealed the correlation between structure and catalytic activity of Fe-based SACs for the first time. By anchoring Fe sites on the reshaped CN support, the efficient combination of SAs-SCs sites with a self pH-adjusting capability was successfully achieved. $FeCN_5$ with both SAs and SCs exhibited excellent performance on multiple contaminant degradation in seconds-level even under high initial pH or anion concentrations. It provides a reference for the precise and low-cost design of catalysts and solves two fundamental problems in the current H_2O_2-AOPs process. More importantly, the actual pH adaptability of the catalyst was disclosed by controlling the pH throughout the reaction, which demonstrated its inhibited activity due to the loss of pH-adjusting capability. It was further addressed by reducing the overexposure of active sites in a novel flow-through Fenton filter constructed from $FeCN_5$ modified CF. The facile and scalable filter showed ultrahigh catalytic activity and sustainability for H_2O_2 activation and pollutant degradation. A minimal Fe leaching, limited energy consumption, easy operation model, and long-term stability under a real wastewater environment also demonstrated this filter design could provide a promising and effective strategy for scale-up application in wastewater treatment.

CRediT authorship contribution statement

Biao Li: Investigation, Methodology, Validation, Formal analysis, Writing – original draft. **Xiaolong Cheng**: Characterization, Writing – review & editing. **Rusen Zou**: Writing – review & editing. **Xiaoyu Yong**: Writing – review & editing. **Chengfang Pang**: Characterization, Writing – review & editing. **Yanyan Su**: Supervision, Resources, Writing – review & editing. **Yifeng Zhang**: Supervision, Resources, Funding acquisition, Writing – review & editing.

Declaration of Competing Interest

The authors declare that they have no known competing financial interests or personal relationships that could have appeared to influence the work reported in this paper.

Acknowledgements

The authors gratefully acknowledge the financial support from China Scholarship Council. This work was financially supported by the Carlsberg Foundation Distinguished Fellowships (CF18-0084, Denmark).

Appendix A. Supporting information

Supplementary data associated with this article can be found in the online version at doi:10.1016/j.apcatb.2021.121009.

References

[1] J. Xu, X. Zheng, Z. Feng, Z. Lu, Z. Zhang, W. Huang, Y. Li, D. Vuckovic, Y. Li, S. Dai, G. Chen, K. Wang, H. Wang, J.K. Chen, W. Mitch, Y. Cui, Organic wastewater treatment by a single-atom catalyst and electrolytically produced H_2O_2, Nat. Sustain. 4 (2020) 233–241.
[2] K. Qian, H. Chen, W. Li, Z. Ao, Y.N. Wu, X. Guan, Single-atom Fe catalyst outperforms its homogeneous counterpart for activating peroxymonosulfate to achieve effective degradation of organic contaminants, Environ. Sci. Technol. 55 (2021) 7034–7043.
[3] Y. Zhao, M. Sun, X. Wang, C. Wang, D. Lu, W. Ma, S.A. Kube, J. Ma, M. Elimelech, Janus electrocatalytic flow-through membrane enables highly selective singlet oxygen production, Nat. Commun. 11 (2020) 6228.
[4] S. Zhang, M. Sun, T. Hedtke, A. Deshmukh, X. Zhou, S. Weon, M. Elimelech, J. H. Kim, Mechanism of heterogeneous fenton reaction kinetics enhancement under nanoscale spatial confinement, Environ. Sci. Technol. 54 (2020) 10868–10875.
[5] Y. Liu, Y. Chen, J. Deng, J. Wang, N-doped aluminum-graphite (Al-Gr-N) composite for enhancing in-situ production and activation of hydrogen peroxide to treat landfill leachate, Appl. Catal. B 297 (2021).
[6] H. Wang, T. Chen, D. Chen, X. Zou, M. Li, F. Huang, F. Sun, C. Wang, D. Shu, H. Liu, Sulfurized oolitic hematite as a heterogeneous Fenton-like catalyst for tetracycline antibiotic degradation, Appl. Catal. B 260 (2020).
[7] J. Zhu, X. Zhu, F. Cheng, P. Li, F. Wang, Y. Xiao, W. Xiong, Preparing copper doped carbon nitride from melamine templated crystalline copper chloride for Fenton-like catalysis, Appl. Catal. B 256 (2019).
[8] D. Guo, Y. Liu, H. Ji, C.C. Wang, B. Chen, C. Shen, F. Li, Y. Wang, P. Lu, W. Liu, Silicate-enhanced heterogeneous flow-through electro-fenton system using iron oxides under nanoconfinement, Environ. Sci. Technol. 55 (2021) 4045–4053.
[9] A. Wang, Z. Zheng, H. Wang, Y. Chen, C. Luo, D. Liang, B. Hu, R. Qiu, K. Yan, 3D hierarchical H_2-reduced Mn-doped CeO_2 microflowers assembled from nanotubes as a high-performance Fenton-like photocatalyst for tetracycline antibiotics degradation, Appl. Catal. B 277 (2020), 119171.
[10] M. Cheng, G. Zeng, D. Huang, C. Lai, Y. Liu, C. Zhang, J. Wan, L. Hu, C. Zhou, W. Xiong, Efficient degradation of sulfamethazine in simulated and real wastewater at slightly basic pH values using Co-SAM-SCS/H_2O_2 Fenton-like system, Water Res. 138 (2018) 7–18.
[11] J. Li, A.N. Pham, R. Dai, Z. Wang, T.D. Waite, Recent advances in Cu-Fenton systems for the treatment of industrial wastewaters: role of Cu complexes and Cu composites, J. Hazard. Mater. 392 (2020), 122261.
[12] F. Liu, Y. Liu, Q. Yao, Y. Wang, X. Fang, C. Shen, F. Li, M. Huang, Z. Wang, W. Sand, Supported atomically-precise gold nanoclusters for enhanced flow-through electro-Fenton, Environ. Sci. Technol. 54 (2020) 5913–5921.
[13] Y. Zhu, R. Zhu, L. Yan, H. Fu, Y. Xi, H. Zhou, G. Zhu, J. Zhu, H. He, Visible-light Ag/AgBr/ferrihydrite catalyst with enhanced heterogeneous photo-Fenton reactivity via electron transfer from Ag/AgBr to ferrihydrite, Appl. Catal. B 239 (2018) 280–289.

[14] H. Cao, J. Wang, J.-H. Kim, Z. Guo, J. Xiao, J. Yang, J. Chang, Y. Shi, Y. Xie, Different roles of Fe atoms and nanoparticles on g-C_3N_4 in regulating the reductive activation of ozone under visible light, Appl. Catal. B 296 (2021).
[15] Y. Yin, W. Li, C. Xu, L. Shi, L.-C. Zhang, Z. Ao, M. Liu, M. Lu, X. Duan, S. Wang, S. Liu, H. Sun, Ultrafine copper nanoclusters and single sites for Fenton-like reactions with high atom utilities, Environ. Sci. Nano 7 (2020) 2595–2606.
[16] H. Zhang, S. Hwang, M. Wang, Z. Feng, S. Karakalos, L. Luo, Z. Qiao, X. Xie, C. Wang, D. Su, Y. Shao, G. Wu, Single atomic iron catalysts for oxygen reduction in acidic media: particle size control and thermal activation, J. Am. Chem. Soc. 139 (2017) 14143–14149.
[17] Y. Long, J. Dai, S. Zhao, Y. Su, Z. Wang, Z. Zhang, Atomically dispersed cobalt sites on graphene as efficient periodate activators for selective organic pollutant degradation, Environ. Sci. Technol. 55 (2021) 5357–5370.
[18] Z. Li, K. Li, S. Ma, B. Dang, Y. Li, H. Fu, J. Du, Q. Meng, Activation of peroxymonosulfate by iron-biochar composites: comparison of nanoscale Fe with single-atom Fe, J. Colloid Interface Sci. 582 (2021) 598–609.
[19] G. Lei, W. Zhao, L. Shen, S. Liang, C. Au, L. Jiang, Isolated iron sites embedded in graphitic carbon nitride (g-C_3N_4) for efficient oxidative desulfurization, Appl. Catal. B 267 (2020).
[20] J. Zhu, H. Li, C. Shan, S. Wang, L. Lv, B. Pan, Trace Co^{2+} coupled with phosphate triggers efficient peroxymonosulfate activation for organic degradation, J. Hazard. Mater. 409 (2021), 124920.
[21] Q. Yan, C. Lian, K. Huang, L. Liang, H. Yu, P. Yin, J. Zhang, M. Xing, Constructing an acidic microenvironment by MoS_2 in heterogeneous Fenton reaction for pollutant control, Angew. Chem. Int. Ed. Engl. 60 (2021) 17155–17163.
[22] S. Wu, D. Yang, Y. Zhou, H. Zhou, S. Ai, Y. Yang, Z. Wan, L. Luo, L. Tang, D. C. Tsang, Simultaneous degradation of p-arsanilic acid and inorganic arsenic removal using M-rGO/PS Fenton-like system under neutral conditions, J. Hazard. Mater. 399 (2020), 123032.
[23] R. Valenzuela, M.C. Fuentes, C. Parra, J. Baeza, N. Duran, S. Sharma, M. Knobel, J. Freer, Influence of stirring velocity on the synthesis of magnetite nanoparticles (Fe_3O_4) by the co-precipitation method, J. Alloy. Compd. 488 (2009) 227–231.
[24] R. Zou, A. Hasanzadeh, A. Khataee, X. Yang, M. Xu, I. Angelidaki, Y. Zhang, Scaling-up of microbial electrosynthesis with multiple electrodes for in situ production of hydrogen peroxide, iScience 24 (2021), 102094.
[25] G. Wang, K. Tang, Y. Jiang, H.R. Andersen, Y. Zhang, Regeneration of Fe (II) from Fenton-derived ferric sludge using a novel biocathode, Bioresour. Technol. 318 (2020), 124195.
[26] D. Trpkov, M. Panjan, L. Kopanja, M. Tadić, Hydrothermal synthesis, morphology, magnetic properties and self-assembly of hierarchical α-Fe_2O_3 (hematite) mushroom-, cube-and sphere-like superstructures, Appl. Surf. Sci. 457 (2018) 427–438.
[27] S. An, G. Zhang, T. Wang, W. Zhang, K. Li, C. Song, J.T. Miller, S. Miao, J. Wang, X. Guo, High-density ultra-small clusters and single-atom Fe sites embedded in graphitic carbon nitride (g-C_3N_4) for highly efficient catalytic advanced oxidation processes, ACS Nano 12 (2018) 9441–9450.
[28] X. Liang, J. Fan, D. Liang, Y. Xu, Y. Zhi, H. Hu, X. Qiu, Surface hydroxyl groups functionalized graphite carbon nitride for high efficient removal of diquat dibromide from water, J. Colloid Interface Sci. 582 (2021) 70–80.
[29] W.D. Oh, V.W.C. Chang, Z. Hu, R. Goei, T.T. Lim, Enhancing the catalytic activity of g-C_3N_4 through Me doping (Me=Cu, Co and Fe) for selective sulfathiazole degradation via redox-based advanced oxidation process, Chem. Eng. J. 323 (2017) 260–269.
[30] L. Peng, X. Duan, Y. Shang, B. Gao, X. Xu, Engineered carbon supported single iron atom sites and iron clusters from Fe-rich Enteromorpha for Fenton-like reactions via nonradical pathways, Appl. Catal. B 287 (2021).
[31] Y. Gao, C. Yang, M. Zhou, C. He, S. Cao, Y. Long, S. Li, Y. Lin, P. Zhu, C. Cheng, Transition metal and metal-Nx codoped MOF-derived Fenton-like catalysts: a comparative study on single atoms and nanoparticles, Small 16 (2020), e2005060.
[32] L. Chen, S. Wang, Z. Yang, J. Qian, B. Pan, Selective interfacial oxidation of organic pollutants in Fenton-like system mediated by Fe(III)-adsorbed carbon nanotubes, Appl. Catal. B 292 (2021).
[33] Y. Yu, Y. Sun, Y. Zhou, A. Xu, Y. Xu, F. Huang, Y. Zhang, The behavior of surface acidity on photo-Fenton degradation of ciprofloxacin over sludge derived carbon: performance and mechanism, J. Colloid Interface Sci. 597 (2021) 84–93.
[34] G. Nie, K. Hu, W. Ren, P. Zhou, X. Duan, L. Xiao, S. Wang, Mechanical agitation accelerated ultrasonication for wastewater treatment: sustainable production of hydroxyl radicals, Water Res. 198 (2021), 117124.
[35] Y. Yin, L. Shi, W. Li, X. Li, H. Wu, Z. Ao, W. Tian, S. Liu, S. Wang, H. Sun, Boosting Fenton-like reactions via single atom Fe catalysis, Environ. Sci. Technol. 53 (2019) 11391–11400.
[36] L. Hu, G. Zhang, M. Liu, Q. Wang, P. Wang, Enhanced degradation of Bisphenol A (BPA) by peroxymonosulfate with Co_3O_4-Bi_2O_3 catalyst activation: effects of pH, inorganic anions, and water matrix, Chem. Eng. J. 338 (2018) 300–310.
[37] R. Yamaguchi, S. Kurosu, M. Suzuki, Y. Kawase, Hydroxyl radical generation by zero-valent iron/Cu (ZVI/Cu) bimetallic catalyst in wastewater treatment: heterogeneous Fenton/Fenton-like reactions by Fenton reagents formed in-situ under oxic conditions, Chem. Eng. J. 334 (2018) 1537–1549.
[38] B. Shen, C. Dong, J. Ji, M. Xing, J. Zhang, Efficient Fe (III)/Fe (II) cycling triggered by MoO_2 in Fenton reaction for the degradation of dye molecules and the reduction of Cr (VI), Chin. Chem. Lett. 30 (2019) 2205–2210.
[39] C. Shan, H. Liu, M. Hua, B. Pan, Enhanced Fenton-like oxidation of As (III) over Ce–Ti binary oxide: a new strategy to tune catalytic activity via balancing bimolecular adsorption energies, Environ. Sci. Technol. 54 (2020) 5893–5901.
[40] J. Liang, X. Duan, X. Xu, K. Chen, Y. Zhang, L. Zhao, H. Qiu, S. Wang, X. Cao, Persulfate oxidation of sulfamethoxazole by magnetic iron-char composites via nonradical pathways: Fe(IV) versus surface-mediated electron transfer, Environ. Sci. Technol. 55 (2021) 10077–10086.
[41] W. Tan, W. Ren, C. Wang, Y. Fan, B. Deng, H. Lin, H. Zhang, Peroxymonosulfate activated with waste battery-based Mn-Fe oxides for pollutant removal: electron transfer mechanism, selective oxidation and LFER analysis, Chem. Eng. J. 394 (2020), 124864.
[42] N. Jiang, H. Xu, L. Wang, J. Jiang, T. Zhang, Nonradical oxidation of pollutants with single-atom-Fe(III)-activated persulfate: Fe(V) being the possible intermediate oxidant, Environ. Sci. Technol. 54 (2020) 14057–14065.
[43] S. Zhu, X. Li, J. Kang, X. Duan, S. Wang, Persulfate activation on crystallographic manganese oxides: mechanism of singlet oxygen evolution for nonradical selective degradation of aqueous contaminants, Environ. Sci. Technol. 53 (2019) 307–315.
[44] Z. Yang, Y. Yan, A. Yu, B. Pan, J.J. Pignatello, Revisiting the phenanthroline and ferrozine colorimetric methods for quantification of Fe (II) in Fenton reactions, Chem. Eng. J. 391 (2020), 123592.
[45] L. Chen, A.N. Alshawabkeh, S. Hojabri, M. Sun, G. Xu, J. Li, A robust flow-through platform for organic contaminant removal, Cell Rep. Phys. Sci. 2 (2021).
[46] L. Zhang, X. Jiang, Z. Zhong, L. Tian, Q. Sun, Y. Cui, X. Lu, J.P. Zou, S. Luo, Carbon nitride supported high-loading Fe single-atom catalyst for activating of peroxymonosulfate to generate $^1O_2$ with 100% selectivity, Angew. Chem. Int. Ed. Engl. 60 (2021) 21751–21755.
[47] S. Yu, Y. Gao, R. Khan, P. Liang, X. Zhang, X. Huang, Electrospun PAN-based graphene/SnO_2 carbon nanofibers as anodic electrocatalysis microfiltration membrane for sulfamethoxazole degradation, J. Memb. Sci. 614 (2020), 118368.
[48] Y. Si, C. Sun, D. Li, F. Yang, C.Y. Tang, X. Quan, Y. Dong, M.D. Guiver, Flexible superhydrophobic metal-based carbon nanotube membrane for electrochemically enhanced water treatment, Environ. Sci. Technol. 54 (2020) 9074–9082.
[49] Y. Xue, Y. Zhang, Y. Zhang, S. Zheng, Y. Zhang, W. Jin, Electrochemical detoxification and recovery of spent SCR catalyst by in-situ generated reactive oxygen species in alkaline media, Chem. Eng. J. 325 (2017) 544–553.